In situ decoration of ZnxCd1−xS with FeP for efficient photocatalytic generation of hydrogen under irradiation with visible light

Zhu, Xianglin; Yu, Sijia; Gong, Xuezhong; Xue, Can

2018

Zhu, X., Yu, S., Gong, X., & Xue, C. (2018). In situ decoration of ZnxCd1−xS with FeP for efficient photocatalytic generation of hydrogen under irradiation with visible light. ChemPlusChem, 83(9), 825-830. doi:10.1002/cplu.201800316

https://hdl.handle.net/10356/105639

https://doi.org/10.1002/cplu.201800316

In-Situ Decoration of FeP on $Zn_xCd_{1-x}S$ for Efficient Photocatalytic Hydrogen Generation under Visible Light Irradiation

Xianglin Zhu, † Sijia Yu, † Xuezhong Gong and Can Xue*

Abstract: FeP as a noble-metal-free catalyst has been successfully decorated onto the $Zn_xCd_{1-x}S$ photocatalyst surface through an in-situ phosphating process. In particular, the 2% FeP/$Zn_{0.5}Cd_{0.5}$S-P sample showed the best activity of 24.45 mmol·h^{-1}·g^{-1} which is over 130 times higher than that of pure $Zn_{0.5}Cd_{0.5}S$ and nearly 1.3 times higher than that of the 1% Pt-loaded $Zn_{0.5}Cd_{0.5}$S-P sample. The apparent quantum yield (AQY) of the 2% FeP/$Zn_{0.5}Cd_{0.5}$S-P was estimated over 10% at a wavelength up to 470 nm. The fluorescence spectra and electrochemical measurement results suggest that the decorated FeP not only reduces the overpotential for H_2 evolution but also promotes the separation of the photogenerated charge carriers through forming heterojunction with $Zn_{0.5}Cd_{0.5}S$, which eventually results in superior activity of the FeP/$Zn_{0.5}Cd_{0.5}$S-P photocatalyst for visible-light-driven hydrogen generation.

Introduction

The over-dependence on the fossil fuels during the past hundred years have caused several serious problems, such as environmental pollution, greenhouse effect and energy shortage.[1-8] Hydrogen energy has attracted attentions of the whole world and been considered as an ideal alternative energy resource, while the way of obtaining cheap hydrogen remains challenging. Since Fujishima found that TiO_2 can split water into H_2 and O_2 under UV light irradiation,[9] photocatalytic techniques have been considered as efficient and clean routes to generate hydrogen gas. TiO_2, as a stable and non-toxic photocatalyst, has been well studied. But due to the wide band gap, it can only absorb UV light which greatly restricts its efficiency for solar hydrogen production [10-14]. As such, it is important to develop photocatalysts having high efficiency under visible-light irradiation.

During the past decades, lots of visible-light-active photocatalysts, including g-C_3N_4,[15, 16] CdS,[17, 18] and $Zn_xCd_{1-x}S$[19-21] etc., have been developed for H_2 generation. Among these photocatalysts, $Zn_xCd_{1-x}S$ is definitely promising for H_2 production. As a ternary chalcogenide, the band gap can be readily tuned through varying the Zn/Cd ratio towards strong visible light response. In addition, $Zn_xCd_{1-x}S$ has lower poison and better stability than pure CdS.[19, 22-24] Although the photocatalytic behaviors of $Cd_xZn_{1-x}S$ have been widely investigated, there are still some serious problems such as rapid recombination of photogenerated charge carriers and high surface overpotential for proton reduction. In order to solve these issues, some strategies, including constructing heterojunction, element doping and loading co-catalyst, have been reported to enhance the activity of $Cd_xZn_{1-x}S$.[23, 25, 26] Previous studies have shown that Pt-loading is the most efficient way to improve the $Zn_xCd_{1-x}S$ performance on photocatalytic H_2 generation because of its appropriate work function and low overpotential for hydrogen evolution reaction (HER). However, the premium price of Pt makes it impossible for large scale use in H_2 evolution. Therefore, the development of earth-abundant noble-metal-free HER catalyst is the key issue for large-scale photocatalytic H_2 production.

In the past decade, some transition metal compounds, such as NiO,[27] NiS_x,[28,29] MoS_2,[30,31] and Mo_2C,[32], have been developed as suitable HER catalysts. Very recently, researchers have found that some metal phosphides, such as Ni_xP_y, Co_xP_y, Cu_3P and FeP, can be used as efficient HER catalysts.[11, 26, 33-38] Thus it is believed that metal phosphides might be good candidates to enhance the photocatalytic activity of $Zn_xCd_{1-x}S$ for H_2 generation.

Herein, in this work, we have successfully deposited FeP catalyst on $Zn_xCd_{1-x}S$ through a two-step in-situ phosphating reaction. The phosphating treated $Zn_xCd_{1-x}S$ samples are denoted as $Zn_xCd_{1-x}S$-P. The light absorption of resulted photocatalysts are tuned by adjusting the Zn/Cd ratio and the loading contents of FeP. In the photocatalytic H_2 production experiments, 2% FeP decorated $Zn_{0.5}Cd_{0.5}$S-P had the best performance, and showed 130 times higher activity than the pure $Zn_{0.5}Cd_{0.5}S$ and nearly 3.5 times higher activity than the 1% Pt/ $Zn_{0.5}Cd_{0.5}$S-P. Our studies demonstrate that FeP-loaded Zn_xCd_{1-x}S-P is promising and highly efficient photocatalysts for visible-light-driven hydrogen generation.

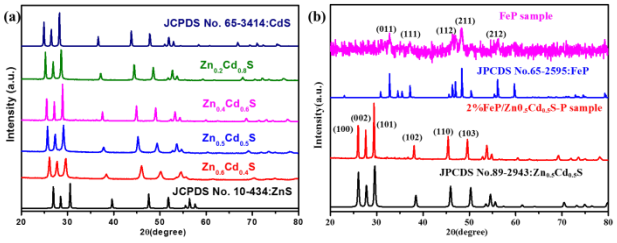

Results and Discussion

Figure 1. (a) XRD patterns of the $Zn_xCd_{1-x}S$; (b) XRD patterns of FeP and 2% FeP/$Zn_{0.5}Cd_{0.5}$S-P.

Dr. X. L. Zhu, S. J. Yu, Dr. X. Z. Gong and Prof. C. Xue*
School of Materials Science and Engineering, Nanyang Technological University, 639798, Singapore
Email: cxue@ntu.edu.sg

[†] These authors contribute equally to this work.

The XRD patterns of $Zn_xCd_{1-x}S$ samples with different Zn/Cd ratios are shown in Figure 1a. The XRD peaks show continuous shift along with increasing Zn/Cd ratio as compared to the peaks of CdS and ZnS, which proves the formation of $Zn_xCd_{1-x}S$ solid solution. The XRD pattern of pure FeP (Figure 1b), synthesized in the absence of $Zn_xCd1_{-x}S$, indicates poor crystallinity of FeP in the present reaction conditions. Nevertheless, we still can distinguish serval typically diffraction peaks corresponding to (001), (111), (112), (211), and (212) planes of FeP (JPCDS No. 65-2595) in the XRD pattern. The XRD pattern of 2% FeP/$Zn_{0.5}Cd_{0.5}S$-P (Figure. 1b) shows the characterization of hexagonal $Zn_{0.5}Cd_{0.5}S$ (JCPDS No. 89-2943). There was no obvious change for $Zn_{0.5}Cd_{0.5}S$ after deposition of FeP, suggesting that the phosphating reaction didn't affect the crystal structure of $Zn_{0.5}Cd_{0.5}S$. But the peaks of FeP can't be distinguished for the FeP/$Zn_{0.5}Cd_{0.5}S$-P sample due to very weak peak intensity of FeP.

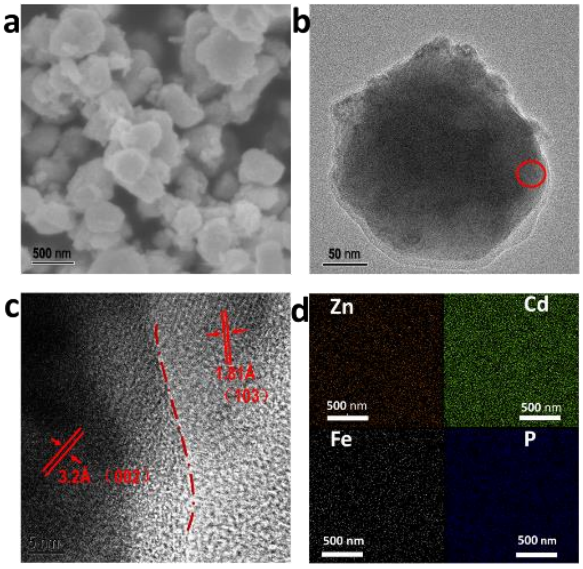

Figure 2. (a) SEM image and (b-c) TEM images of the as prepared the 2% FeP/$Zn_{0.5}Cd_{0.5}S$-P; (d) Elemental mapping images of the red marking circle area in (b), showing the presence of Zn, Cd, Fe and P, respectively.

The morphology of the 2% FeP/$Zn_{0.5}Cd_{0.5}S$-P sample was characterized with SEM and TEM. As shown in Figure 2, the sample appears as irregular spheres with diameters of 300-500 nm. In the HRTEM image (Figure 2c and Figure S1) of the FeP/$Zn_{0.5}Cd_{0.5}S$-P interface, we can identify two characteristic lattice fringes of 3.20 Å and 1.81 Å, corresponding to the (002) plane of $Zn_{0.5}Cd_{0.5}S$ and (103) plane of FeP.[26, 38] The elemental mapping images (Figure 2d) reveal that all elements, Zn, Cd, Fe and P, are homogeneously distributed, suggesting uniform distribution of FeP on the $Zn_{0.5}Cd_{0.5}S$ surface. The particle size of FeP is about 5 nm according to the TEM image (Figure S2).

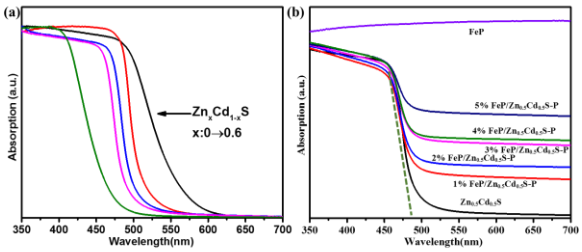

Figure 3. The absorption spectra of (a) different $Zn_xCd_{1-x}S$ samples and (b) pure FeP and $Zn_{0.5}Cd_{0.5}S$-P with different loading amount of FeP.

The absorption spectra of $Zn_xCd_{1-x}S$ (Figure 3a) show that the absorption band gradually shifts toward to UV region with increasing Zn content. The absorption spectra of the $Zn_{0.5}Cd_{0.5}S$-P samples with different loading amount of FeP (Figure 3b) indicates that the absorption edge of $Zn_{0.5}Cd_{0.5}S$ has no obvious change.

The photocatalytic activities for H_2 generation over the prepared samples are shown in Figure 4. The photocatalytic activities of $Zn_xCd_{1-x}S$ are dependent on the Zn/Cd ratio. By comparing all $Zn_xCd_{1-x}S$ samples loaded with 2% FeP (Figure 4a), we found that the best performance was presented by the sample with equal molar content of Zn and Cd (2% FeP/$Zn_{0.5}Cd_{0.5}S$-P). Indeed, as shown in Figure 4b, for all $Zn_xCd_{1-x}S$ samples, upon loading with 2% FeP catalyst, the activities were remarkably enhanced. We note that the 2% FeP loading amount is optimal based on the comparison test of different loading percentage of FeP (Figure 4c-d). The average H_2 evolution rate for 2% FeP-loaded $Zn_{0.5}Cd_{0.5}S$-P is about 24.45 $mmol \cdot h^{-1} \cdot g^{-1}$, which is over 130 times higher than that of the pure $Zn_{0.5}Cd_{0.5}S$ sample, and is about 1.3 times higher than that of the 1% Pt-loaded $Zn_{0.5}Cd_{0.5}S$-P. These results demonstrate that FeP is a promising catalyst and comparable to Pt for photocatalytic H_2 generation. We also investigated the photocatalytic activity of the phosphating $Zn_xCd_{1-x}S$ without Fe and the result are shown in Figure S3. The activity of the phosphating $Zn_xCd_{1-x}S$-P were 3.7-6.2 times of the pure $Zn_xCd_{1-x}S$. This indicates the phosphating process benefited the photocatalytic activity. But the activity of the phosphating $Zn_xCd_{1-x}S$-P samples are still far lower than the FeP/$Zn_xCd_{1-x}S$-P samples by comparing Figure S3 with Figure 4d. Thus we believe that decorated FeP catalyst is the dominating factor responsible to the greatly enhanced photocatalytic activities for hydrogen generation.

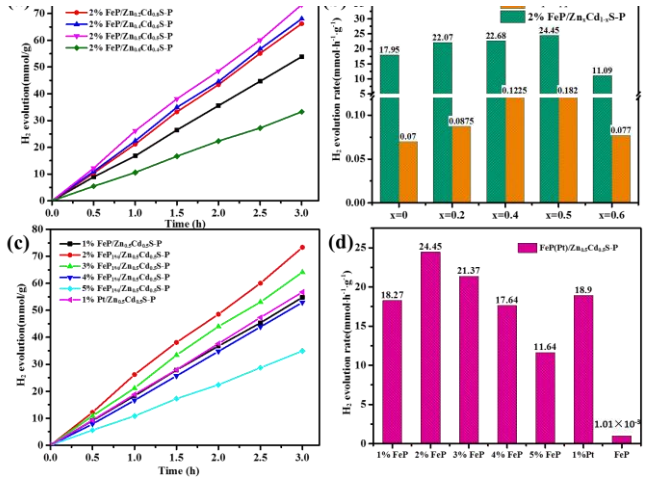

Figure 4. Photocatalytic H_2 evolution experiments (a), (b) 2% FeP/$Zn_xCd_{1-x}S$-P, and (c), (d) $Zn_{0.5}Cd_{0.5}S$-P with different amount of FeP or 1%Pt.

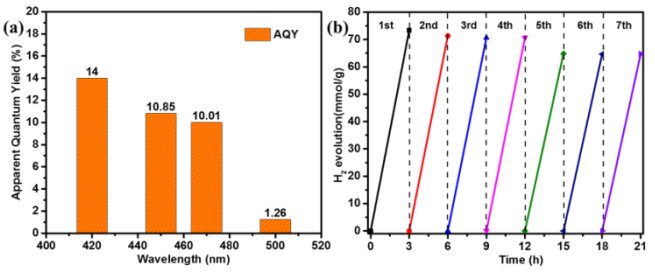

Figure 5. (a) The apparent quantum yield at different wavelength, (b) Cycling photocatalytic H_2 evolution tests

Besides the photocatalytic H_2 evolution rate, the apparent quantum yield (AQY) and stability are another two important factors to evaluate the quality of photocatalysts. For the 2% FeP-loaded $Zn_{0.5}Cd_{0.5}S$-P, the AQY at 420 nm, 450 nm, 470 nm and 500 nm were estimated as 14.00 %, 10.85%, 10.01% and 1.26% respectively (Figure 5a). The low AQY at 500 nm might be ascribed to the weak absorption of $Zn_{0.5}Cd_{0.5}S$ at 500 nm. The cycling experiment result (Figure 5b) showed that the 2% FeP/$Zn_{0.5}Cd_{0.5}S$-P sample retained 90% activity after 7 cycles, which indicates very good stability of the sample for photocatalytic H_2 production.

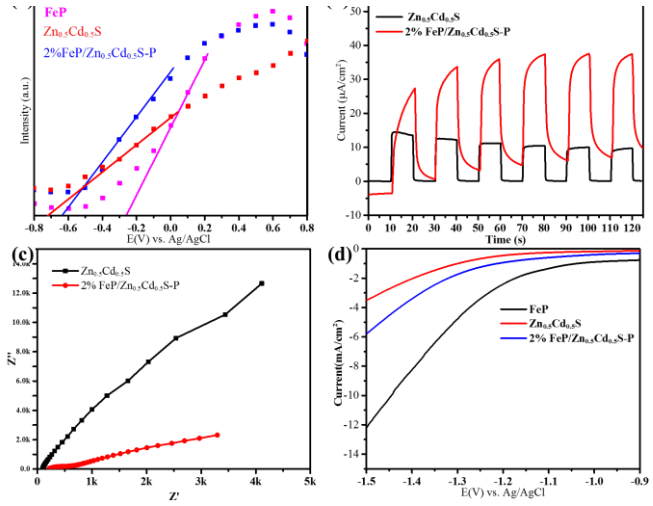

Figure 6. Electrochemical characterizations of the catalysts in 0.5 M Na_2SO_4 solution (a) Mott–Schottky plots of the FeP, $Zn_{0.5}Cd_{0.5}S$ and 2% FeP/$Zn_{0.5}Cd_{0.5}S$-P, (b) Photocurrent results of the $Zn_{0.5}Cd_{0.5}S$ and 2% FeP/$Zn_{0.5}Cd_{0.5}S$-P at 0 V vs. Ag/AgCl, (c) EIS Nyquist plots of the $Zn_{0.5}Cd_{0.5}S$ and 2% FeP/$Zn_{0.5}Cd_{0.5}S$-P at 0 V vs. Ag/AgCl, (d) Electrochemical H_2 evolution tests of the FeP, $Zn_{0.5}Cd_{0.5}S$ and 2% FeP/$Zn_{0.5}Cd_{0.5}S$-P.

In order to investigate the charge transfer for the prepared samples, we have carried out electrochemical characterizations. Figure 6a shows the results of Mott- Schottky (MS) test, which has been widely used to estimate the flat band potential of semiconductors. The MS plot of $Zn_{0.5}Cd_{0.5}S$ shows a positive slope, indicating typical n-type semiconductor feature. It is known that the flat band potential for n-type semiconductors is close to their conduction band (CB).[40] From Figure 6a, we can estimate the flat band potential of FeP, $Zn_{0.5}Cd_{0.5}S$ and 2% FeP/$Zn_{0.5}Cd_{0.5}S$-P as -0.27 V, -0.71V and -0.63V, respectively. The results suggest that $Zn_{0.5}Cd_{0.5}S$ has more negative CB position than FeP, and the heterojunction formation between FeP and $Zn_{0.5}Cd_{0.5}S$ lowers the flat band potential level of $Zn_{0.5}Cd_{0.5}S$ and enables electron transfer from $Zn_{0.5}Cd_{0.5}S$ to FeP to promote charge separation. Consistently, in the photoelectrochemical tests (Figure 6b), the 2% FeP/$Zn_{0.5}Cd_{0.5}S$-P sample shows much higher photocurrent intensity than the pure $Zn_{0.5}Cd_{0.5}S$.

For semiconductor photocatalysts, most of photogenerated charge carriers can't separate in time due to poor conductivity, and high overpotential. Here, we have checked the sample conductivities by using electrochemical impedance spectroscopy (EIS). According to Figure 6c, the 2% FeP/$Zn_{0.5}Cd_{0.5}S$-P sample presents a much smaller radius than the pure $Zn_{0.5}Cd_{0.5}S$ sample, suggesting better conductivity for 2% FeP/$Zn_{0.5}Cd_{0.5}S$-P, which would be also beneficial to the photocatalytic activities [41]. The linear sweep voltammetry (LSV) test is used to explore the electrocatalytic activity of the sample for HER without light irradiation. Typically, smaller onset potential or bigger current at the same potential would be corresponding to higher efficiency for HER.[42] As shown in Figure 6d, pure FeP exhibit smaller onset potential with high current, suggesting its good activity in HER. Consistently, loading FeP onto $Zn_{0.5}Cd_{0.5}S$ also improved the HER activity as compared to the pure $Zn_{0.5}Cd_{0.5}S$.

The charge transfer process can be further verified by the fluorescence spectra. As shown in Figure 7, under excitation at 380nm, the emission intensity of $Cd_{0.5}Zn_{0.5}S$ is obviously quenched upon loading FeP. This result suggests that the surface FeP can facilitate charge transfer from $Cd_{0.5}Zn_{0.5}S$ so as to suppress the charge recombination, which supports the better activity of FeP/$Zn_{0.5}Cd_{0.5}$S-P photocatalysts.

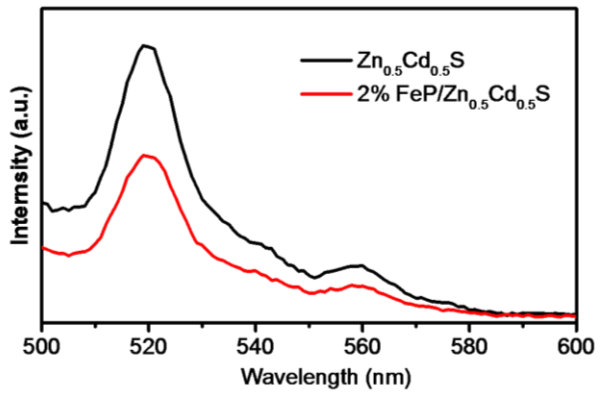

Figure 7. Fluorescence spectra of $Zn_{0.5}Cd_{0.5}S$ and 2% FeP/$Zn_{0.5}Cd_{0.5}$S under excitation at 380nm.

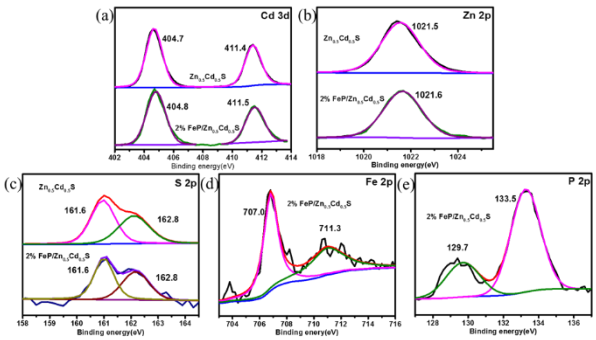

Figure 8. XPS spectra of (a) Cd 3d, (b) Zn 2p. (c) S 2p, (d) Fe 2p, and P 2p for the $Zn_{0.5}Cd_{0.5}S$ and 2% FeP/$Zn_{0.5}Cd_{0.5}$S samples.

In addition, we have used X-ray photoelectron spectroscopy (XPS) to further characterize the FeP/$Zn_{0.5}Cd_{0.5}$S-P heterojunction. As shown in Figure 8, the binding energies of Cd and Zn slightly shift toward higher energy, which can be attributed to the effect of heterojunction formation at the FeP/$Zn_{0.5}Cd_{0.5}$S-P interface.[43] For the XPS of Fe, there are two peaks at 707.0 and 711.3 eV corresponding to Fe $2p_{3/2}$ in FeP. For the XPS of P 2p, the peak at 129.7 eV represents the negatively charged phosphide ion in FeP, while another peak at 133.5eV is attributed to the surface PO_4^{3-} caused by oxidation of phosphor.[37,38] The XPS results prove the existing of FeP and the shifts of XPS binding energy also indicated the formation of heterojunction between FeP and $Zn_{0.5}Cd_{0.5}$S-P.

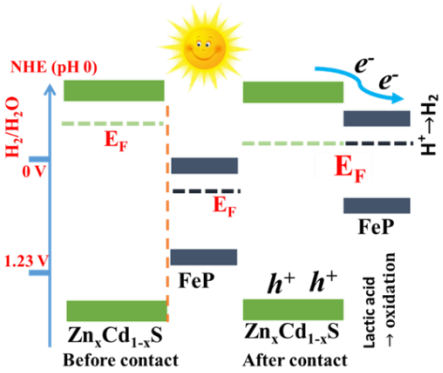

Figure 9. Schematic illustration of charge transfer in the photocatalytic process over the FeP/Zn_xCd_{1-x}S-P sample.

In summary, we have prepared highly efficient noble-metal-free FeP/Zn_xCd_{1-x}S photocatalysts through an in-suit phosphating method. The decorated FeP as catalyst and greatly enhanced the photocatalytic activity of Zn_xCd_{1-x}S for H_2 generation. The 2% FeP/$Zn_{0.5}Cd_{0.5}$S-P showed the best activity of 24.45 $mmol \cdot h^{-1} \cdot g^{-1}$ which is over 130 times of the pure $Zn_{0.5}Cd_{0.5}$S, and even better than that of the 1% Pt-loaded $Zn_{0.5}Cd_{0.5}$S-P. The proposed mechanism of the photocatalytic process is shown in Figure 9 based on the characterization results, which indicated that FeP can serve as an excellent HER catalyst for Zn_xCd_{1-x}S and the decoration of FeP not only lows the overpotential for H_2 evolution but also promotes the separation of photogenerated charge carriers owing to the formed FeP/$Zn_{0.5}Cd_{0.5}$S-P heterojunction. The excellent performance of FeP/Zn_xCd_{1-x}S-P indicates that FeP is a promising noble-metal-free HER catalyst and can be also potentially used in other photocatalytic systems for hydrogen generation because of its high activity and low-cost.

Experimental Section

Materials: Zinc acetate ($ZnC_4H_6O_4 \cdot 2H_2O$, Sigma, 98%), Cadmium acetate ($CdC_4H_6O_4 \cdot 2H_2O$, Sigma, 98%), Sodium sulfide (Na_2S, Sigma, 98%), Sodium hypophosphite (NaH_2PO_2, Sigma, 98%), Iron (III) chloride hexahydrate ($FeCl_3 \cdot 6H_2O$, Sigma, 98%).

Synthesis of photocatalysts: The Zn_xCd_{1-x}S samples were synthesized through a modified co-precipitation followed by high temperature annealing.[39] Typically, 2 mmol precursors, including zinc acetate and cadmium acetate, were dissolved into 15 mL deionized water, then 5 mL of 0.5 M sodium sulfide solution was dropped into the above solution under stirring. After vigorous stirring for 2h at room temperature, the precipitation was collected by centrifugation and washed with deionized water and absolute ethanol. The product was dried at 60℃ in vacuum, and annealed at 500° C (ramping rate 5° C/min) for 2 hours in Ar atmosphere.

The FeP/Zn_xCd_{1-x}S-P samples (with different weight percentages) were prepared by two-step in-situ phosphating reaction. Firstly, 200 mg Zn_xCd_{1-x}S powder was suspended in 20 mL deionized water, and then certain amount of 10 mM $FeCl_3$ solution was dropped into the Zn_xCd_{1-x}S suspension. After stirring for one hour, 1 mL of 1 M NaOH solution was dropped into the above solution with further stirring for 3 hours. The obtained precipitate, as $Fe(OH)_x/Zn_xCd_{1-x}$S, was separated by high speed centrifugation and then was washed with deionized water and absolute

ethanol, dried, and placed in a crucible together with 0.5 g NaH_2PO_2. Then the crucible was put into a tube furnace with NaH_2PO_2 located at the upstream side and annealed at 350°C (ramping rate 2°C/min) in Ar atmosphere.

The 1% Pt-loaded $Zn_{0.5}Cd_{0.5}S$ (weight percentage) was prepared through a simple chemical reduction method. Typically, certain amount of K_2PtCl_6 solution (1 mg Pt/mL) was dropped into 100 mg $Zn_{0.5}Cd_{0.5}S$ under grinding, followed by dropwise adding 0.5 mL of iced $NaBH_4$ solution (1 M) under continuous grinding for 5 min. Finally, the sample was dried at 80°C.

Characterization: The X-ray diffraction (XRD) patterns of samples were recorded on a Bruker D8 ADVANCE powder diffractometer using Cu-K radiation (λ=0.1542 nm). Transmission electron microscopy (TEM) measurements were carried out by JEM-2010 microscope. The absorption spectra were obtained on a UV–vis Spectrophotometer (UV-2501, Shimadzu).

Photocatalytic experiments: The photocatalytic H_2 evolution experiment was carried out in a 50 mL quartz reactor which is equipped with a rubber stopper to keep the system sealing. A 300-W xenon arc lamp coupled with a 420-nm cut-off filter was used to as the visible light source source with irradiation area of 3 cm^2 and light intensity of 390 $mW \cdot cm^{-2}$. The quartz reactor was irradiated from the side direction. The monochromatic light intensities for different wavelength are 420 nm: 2.03 $mW \cdot cm^{-2}$; 450 nm: 2.40 $mW \cdot cm^{-2}$; 470 nm: 3.73 $mW \cdot cm^{-2}$; 500 nm: 7.39 $mW \cdot cm^{-2}$. The reaction temperature was maintained as 25° C. In a typical photocatalytic H_2 production process, 10 mg of catalysts was dispersed in 10 mL of solution containing 9 mL water and 1 mL lactic acid (sacrificial agent) with constant stirring. Before the photocatalytic experiments, the reaction system was degassed with pure N_2 for 30 minutes to remove O_2. A gas chromatography with TCD detector was used to analyze the H_2 amount.

Electrochemical measurements: A typical three-electrode system, containing an Ag/AgCl (in 3 M KCl solution) reference electrode and a carbon rod as the counter electrode was used and controlled by an Autolab electrochemical analyzer. For the preparation of working electrode, 10.0 mg of catalyst was suspended into a mixed solvent containing 2 mL absolute ethanol and 2 mL deionized water with sonication for about 30 min to form a homogeneous ink, and then the electrode was prepared by dropping 100 μL ink onto 1cm × 2 cm FTO glass followed by drying at 80 °C.

Acknowledgements

The authors acknowledge the financial support from NTU seed funding for Solar Fuels Laboratory, Singapore MOE AcRF-Tier1 (2016-T1-002-087, RG 120/16) and MOE AcRF-Tier2 (MOE2016-T2-2-056).

Conflict of interest

The authors declare no conflict of interest.

Keywords: photocatalysis • hydrogen generation • metal phosphide • HER catalyst • heterojunction

[1] I. K. Konstantinou, T. A. Albanis, *Appl. Catal., B* 2004, 49, 1-14.
[2] A. Kudo, Y. Miseki, *Chem. Soc. Rev.* 2009, 38, 253-278.
[3] P. Wang, B. B. Huang, X. Y. Qin, X. Y. Zhang, Y. Dai, J. Y. Wei, M.H. Whangbo, *Angew. Chem. Int. Ed.* 2008, 47, 7931-7933.
[4] S. Linic, P. Christopher, D. B. Ingram, *Nat. Mater.* 2011, 10, 911-921.
[5] X. D. Chen, S. M. Mao, *Chem. Rev*. 2007, 107, 2891-2959.
[6] Z. Wang, S. W. Cao, S. C. J. Loo, C. Xue, *CrystEngComm* 2013, 15, 5688-5693.
[7] Y. P. Yuan, S. W. Cao, L. S. Yin, L. Xu, C. Xue, *Int. J. Hydrogen Energy* 2013, 38, 7218-7223.
[8] H. Maleki, N. Hüsing, *Appl. Catal., B* 2018, 221, 530-555.
[9] A. Fujishima, K. Honda, *Nature* 1972, 238, 37-38.
[10] Y. L. Liu, M. F. Zhang, C.-H. Tung, Y. F. Wang, *ACS Catal.* 2016, 6, 8389-8394.
[11] X. Z. Yue, S. S. Yi, R. W. Wang, Z. T. Zhang, S. L. Qiu, *Nanoscale* 2016, 8, 17516-17523.
[12] W. L. Yang, Y. Liu, Y. Hu, M. J. Zhou, H. S. Qian, *J. Mater. Chem.* 2012, 22, 13895-13898.
[13] X. L. Zhu, P. Wang, B. B. Huang, X. C. Ma, X. Y. Qin, X. Y. Zhang, Y. Dai, *Appl. Catal., B 2016*, 199, 315-322.
[14] X. L. Liu, X. Z. Liang, P. Wang, B. B. Huang, X. Y. Qin, X. Y. Zhang, Y. Dai, *Appl. Catal., B*, 2017, 203 282-288.
[15] Q. Gu, Z. W. Gao, C. Xue, *Small* 2016, 12, 3543-3549.
[16] D. Zhang, Y. L. Guo, Z. K. Zhao, *Appl. Catal., B* 2018, 226, 1-9.
[17] Q.-X. Peng, D. Xue, S.-Z. Zhan, C.-L. Ni, *Appl. Catal., B* 2017, 219, 353-361.
[18] X. L. Zhu, P. Wang, Q. Q. Zhang, Z. Y. Wang, Y. Y. Liu, X. Y. Qin, X. Y. Zhang, Y. Dai, B. B. Huang, *RSC Adv.* 2017, 7, 44626-44631.
[19] S. Ghosh, S. Sarkar, B.K. Das, D. Sen, M. Samanta, K. K. Chattopadhyay, *Phys. Chem. Chem. Phys.* 2017, 19, 29998-30009.
[20] X. Liu, X. Q. Li, L. X. Qin, J. Mu, S.-Z. Kang, *J. Mater. Chem. A* 2017, 5, 14682-14688.
[21] J. M. Chen, J. Y. Chen, Y. W. Li, *J. Mater. Chem. A* 2017, 5, 24116-24125.
[22] Y. Jin, H. Y. Zhang, C. Song, L. F. Wang, Q. Y. Lu, F. Gao, *Sci. Rep.* 2016, 6, 29997.
[23] X.-F. Zhang, Y. Z. Chen, Y. Feng, X. G. Zhang, J. H. Qiu, M. M. Jia, J. F. Yao, *J. Alloys Compd.* 2017, 705, 392-398.
[24] Z. W. Mei, B. K. Zhang, J. X. Zheng, S. S. Yuan, Z. Q. Zhuo, X. G. Meng, Z. H. Chen, K. Amine, W. L. Yang, L. W. Wang, W. Wang, S. F. Wang, Q. H. Gong, J. Li, F. S. Liu, F. Pan, *Nano Energy* 2016, 26, 405-416.
[25] Y. G. Chen, S. Zhao, X. Wang, Q. Peng, R. Lin, Y. Wang, R. G. Shen, X. Cao, L. B. Zhang, G. Zhou, J. Li, A. D. Xia, Y. D. Li, *J. Am. Chem. Soc.* 2016, 138, 4286-4289.
[26] D. S. Dai, H. Xu, L. Ge, C. C. Han, Y. Q. Gao, S. S. Li, Y. Lu, *Appl. Catal. B* 2017, 217, 429-436.
[27] J. N. Liu, Q. H. Jia, J. L. Long, X. X. Wang, Z. W. Gao, Q. Gu, *Appl. Catal. B* 2017, 222, 35-43.
[28] L. S. Yin, Y. P. Yuan, S. W. Cao, Z. Y. Zhang, C. Xue, *RSC Adv.* 2017, 4, 6127-6132.
[29] J. Q. Wen, J. Xie, H. D. Zhang, A. P. Zhang, Y. J. Liu, X. B. Chen, X. Li, *ACS Appl. Mater. Inter.* 2017, 9, 14031-14042.
[30] J. Z. Chen, X.-J. Wu, Y. Gong, Y. H. Zhu, Z. Z. Yang, B. Li, Q. P. Lu, Y. F. Yu, S. K. Han, Z. C. Zhang, Y. Y. Zong, Y. Han, L. Gu, H. Zhang, *J. Am. Chem. Soc.* 2017, 139 , 8653-8660.
[31] Q. Gu, H. Sun, Z. Xie, Z. W. Gao, C. Xue, *App. Surf. Sci.* 2017, 396, 1808-1815.
[32] X. Z. Yue, S. S. Yi, R. W. Wang, Z. T. Zhang, S. L. Qiu, *J. Mater. Chem. A* 2017, 5, 10591-10598.
[33] Z. C. Sun, M. S. Zhu, M. Fujitsuka, A. J. Wang, C. Shi, T. Majima, *ACS Appl. Mater. Inter.* 2017, 9, 30583-30590.
[34] Z. X. Qin, Y. B. Chen, Z. X. Huang, J. Z. Su, L. J. Guo, *J. Mater. Chem. A* 2017, 5, 19025-19035.
[35] B. C. Qiu, Q. H. Zhu, M. Y. Xing, J. L. Zhang, *Chem. Commun.* 2017, 53, 897-900.
[36] J. Q. Tian, Q. Liu, N. Y. Cheng, A. M. Asiri, X. P. Sun, *Angew. Chem. Int. Ed. Engl.* 2014, 53, 9577-9581.
[37] C. Y. Son, I. H. Kwak, Y. R. Lim, J. Park, *Chem. Commun.* 2016, 52, 2819-2822.
[38] H. Q. Cheng, X.-J. Lv, S. Cao, Z. Y. Zhao, Y. Chen, W.-F.Fu, *Sci. Rep.* 2016, 6, 19846.
[39] J. Zhang, J. G. Yu, M. Jaroniec, J. R. Gong, *Nano Lett.* 2012, 12, 4584-4589.
[40] X. L. Yu, R. F. Du, B. Y. Li, Y. H. Zhang, H. J. Liu, J. H. Qu, X. Q. An, *Appl. Catal., B* 2016, 182, 504-512.

[41] B. Han, S. Q. Liu, N. Zhang, Y.-J. Xu, Z.-R. Tang, *Appl. Catal. B* 2017, 202, 298-304.
[42] Z. Y. Lin, J. L. Li, Z. Q. Zheng, L. H. Li, L. L. Yu, C. X. Wang, G. W. Yang, *Adv. Energy Mater.* 2016, 6, 1600510.
[43] H. T. Zhao, R. R. Sun, X. Y. Li, X. Sun, *Mater. Sci. Semicond. Process.* 2017, 59, 68-75.

Decoration of FeP on the $Zn_xCd_{1-x}S$ photocatalysts greatly enhances their activities for hydrogen generation under visible light irradiation because FeP improves charge separation and lowers overpotantial for H_2 evolution.

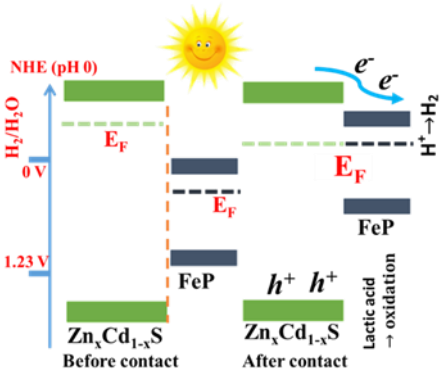

*X. L. Zhu, X. Z. Gong, S. J. Yu and X. Cue**

In-Situ Decoration of FeP on $Zn_xCd_{1-x}S$ for Efficient Photocatalytic Hydrogen Generation under Visible Light Irradiation